

Article

Spatial Magnetic-Field Description Method Aimed at 2×25 kV Auto-Transformer Power Supply System in High-Speed Railway

Yunchuan Deng , Ke Huang, Dongdong Su and Zhigang Liu * 

School of Electrical Engineering, Southwest Jiaotong University, Chengdu 610031, China; dengdeng_10@sina.com (Y.D.); hk1328170662@sina.com (K.H.); 18482189844@163.com (D.S.)

* Correspondence: liuzg_cd@126.com

Received: 14 May 2018; Accepted: 8 June 2018; Published: 19 June 2018



Abstract: Complete and accurate spatial magnetic field description is the premise of effectively assessing the power supply capability of a high-speed railway (HSR). Its evaluation indicators are the current distributions and the integrated impedance of traction network. This paper proposes a spatial magnetic-field description method for the auto-transformer (AT) power supply system. Due to the limitations of previous approaches, all the real loop circuits of the AT system are considered for structuring a loop circuit matrix. At first, different description processes are divided, respectively, into those for the right side and the left side of the load. Then, considering that two types of return conductors exist in an AT system, a certain current ratio deduced in existing studies is introduced. As the introduced current ratio of the left side of the load is approximate, an iterative scheme is adopted. By constantly adjusting current ratio to satisfy a constraint condition of circuit voltages, accurate traction network impedance is obtained. Last, in order to verify the effectiveness of the proposed description method, two real-life experiments in a Chinese HSR line are performed, which indicate that the proposed method can not only directly reflect complete and accurate current distribution, but also deduce the exact traction network integrated impedance.

Keywords: high-speed railway (HSR); spatial magnetic-field description method; auto-transformer (AT) power supply; real loop circuits; traction network integrated impedance; current distribution

1. Introduction

China's high-speed trains (HST) has been developed rapidly in recent years. As an important system of a high-speed railway (HSR), the traction network directly influences the reliable power supply of trains. Focusing on the traction network, the short-circuit influence and the voltage loss are two important parts of the power-supply capability. In the actual operation of an HSR, the short-circuit catenary fault is easily caused by an accidental collision of a bird with the conductor, an internal fault of the train, etc. The voltage loss of the traction network is heavily influenced by the power supply mode of the traction network. Therefore, it is necessary to effectively assess the power supply capability of the traction network on the basis of establishing an accurate traction network mathematical model. The power supply capability is reflected by the traction network integrated impedance. Performing complete and accurate spatial magnetic field description is a premise for obtaining exact traction network integrated impedance.

Aiming at the traction network, many scholars have tried to establish its mathematical model by applying multi-conductor transmission-line (MTL) theory. Existing models mainly include a unified chain circuit model applicable to different power supply modes [1,2], harmonic models [3,4], MTL models of various traction networks, e.g., an auto-transformer (AT) supply system and a novel

cable supply system [5–7]. Some application studies have been also done. In [5], the magnetic fields and harmonics in the surroundings of the AT traction network were analyzed. In [8,9], the electromagnetic compatibility of the traction network was assessed. In [10], a strategy for suppressing low-frequency oscillation has been proposed and its effectiveness was proved by a model simulating a HST-traction network electrical coupling system. Aimed at the AT system with protection wire, a merge process of protection wire and rail was performed and the rail potential was analyzed with a decoupling method in [11]. Moreover, many researchers have studied the electromagnetic interference caused by a common lightning strike [12], pantograph detachment arc [13], etc. Meanwhile, with the help of theoretical analyses, software simulations or experimental measurements, models of the arc, HST, etc., are established and introduced into various traction network mathematical models to analyse accurately interference sources such as arcing phenomenon, vehicle body over-voltages, pantograph over-voltages [14,15].

Focusing on railway lines on special roads such as stations, tunnels and viaducts, some electromagnetic transient models were also studied [16–20]. In [18], the traction network system of the viaduct path is equivalent to the lumped parameter model and the viaduct's electrical coupling is considered in modelling. In [19,20], the influences of the arc-burning phenomenon of insulated rail joints were investigated by state-space model analyses and chain modelling simulations, respectively. Combined with MTL theory, the inductive and capacitive couplings of conductors in the station path are reflected in the chain model of the traction network. Nevertheless, in the aspect of spatial magnetic field description, the application study of traction network models has been insufficient [21].

According to basic electromagnetic theory, obtaining complete and accurate current distribution is the premise for realizing complete and accurate spatial magnetic field description. For the AT system that is widely applied to HSR, some scholars have investigated the current distributions by equaling the AT system to a simple topology [22–24]. Compared with studies that regard the AT system as an ideal system [22,23], In [24], a derivation method considering the fact that rail current is not null at the road of a long loop circuit was proposed. Nevertheless, because many real conductors are merged when the AT system is equaled to a simple topology, only the current distribution coefficient of a merged conductor can be obtained.

In order to study the spatial magnetic field description of the AT system, obtaining the exact current distribution coefficient of each conductor is necessary. Corresponding studies are very few so far and involve the traction network mathematical model based on MTL theory [21].

In the existing traction network mathematical model based on MTL theory, the earth is generally taken as reference conductor. However, this causes some limitations in the spatial magnetic field description. Taking the simple direct power supply system as an example, the limitations are illustrated as follows.

As shown in Figure 1, because the earth is assumed as the reference conductor, each fundamental spatial magnetic field unit (namely loop circuit) is structured by the earth and the other traction network conductor at first. For the earth, this structures Loop circuit 1, Loop circuit 2, Loop circuit 3, Loop circuit 4 with a carrier cable, contact cable, rail and return cable, respectively. For each loop circuit, only after assuming that the current of the reference conductor has the same amplitude and the opposite direction as the other conductor, can the self and mutual flux linkage be calculated. That is, the rail current is composed of four parts, and the four parts respectively have the same amplitude and the opposite direction as the currents of the carrier cable, contact cable, rail and return cable.

To begin with, the traction substation shown in Figure 1 can be seen as an excitation source of the traction network. The carrier cable and contact cable are used for transferring currents from the excitation source to the HST, and the rail, return cable and the earth are used for returning currents from the HST to the excitation source. Therefore, the carrier cable and contact cable are transmission conductors, while the rail, return cable and earth are return conductors. Because the real traction network loop circuit is constituted by the transmission conductor and the return conductor, Loop circuit 3 and Loop circuit 4 are assumed to be loop circuits. Hence, the spatial magnetic field description is not starting from the reality of traction network in the conventional method.

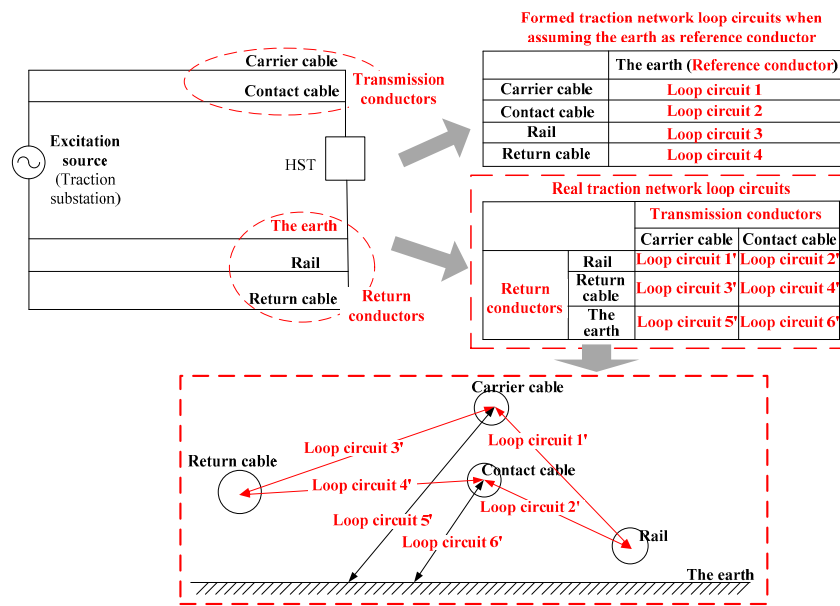


Figure 1. Diagram of the formed loop circuits when assuming the earth as the reference conductor and all the real loop circuits for a simple direct power supply system.

In addition, since the currents of Loop circuits 3–4 are not generated by the excitation source, the deduced interlinkage flux of Loop circuits 3–4 and Loop circuits 1–2 is different from the interlinkage flux of the real loop circuits. This leads to the imprecise description of the spatial magnetic field.

Furthermore, it can be demonstrated from Figure 1 that the currents of Loop circuits 1–4 are namely the currents of the carrier cable, contact cable, catenary, rail and return cable. However, the currents of Loop circuits 1–4 are only the partial currents of the carrier cable, contact cable, catenary, rail and return cable in actuality. Taking the carrier cable current an example, this includes not only the current of Loop circuit 1, but also the currents of the loop circuit that is constituted by carrier cable and rail and the loop circuit that is constituted by the carrier cable and return cable. So, the conventional approach lacks the complete description.

Finally, according to the conventional approach, the sum of currents of Loop circuits 3–4 is assumed to be equal to that of Loop circuits 1–2 in Figure 1. Obviously, the earth’s own current is ignored in this relation. The actual relation should be that the sum of the currents of Loop circuits 3–4 and the self-current of the earth is equal to that of Loop circuits 1–2. Neglecting the earth self-current also illustrates the incompleteness of the conventional approach.

For the reason that the real loop circuit is composed of the transmission conductor and the return conductor, the total number of real loop circuits in a simple direct power supply system is six, including Loop circuit 1', Loop circuit 2' . . . Loop circuit 6' of Figure 1. If all the real loop circuits are considered in the calculation of traction network current distribution, it is possible to gain a complete and accurate spatial magnetic field description. In addition, as for the AT system, two types of return conductors exist in it. The electrical structure of the AT system is relatively more complex than that of a simple direct power supply system. Considering that there is also no related research that considers the detailed electrical structure of the AT system so far, it is necessary to have a complete and accurate spatial magnetic field description of AT system, after considering all the real traction network loop circuits and the power supply characteristics of the AT system.

In this paper, a spatial magnetic field description method of the AT system is presented. It not only adopts the traction network mathematical model based on MTL theory, but also combines the actuality of the detailed electrical structure of AT system. Starting from fundamental considerations in theory, the traditional assumption that the earth is the reference conductor of all the conductors is canceled and all the real traction network loop circuits are considered as fundamental spatial magnetic field

units. Considering that two types of return conductors exist and they have different voltages to the transmission conductor in the AT system, a fundamental relation formula of return conductor current and transmission conductor current is introduced. On this basis, an iterative calculation approach is adopted to realize the exact spatial magnetic field unit.

The rest of this paper is organized as follows. Section 2 shows the analysis of an AT double-track system based on MTL theory. Then, the common situation that the load is running in the up traction network or the down traction network is taken as an example to illustrate the description processes of the proposed description method in Section 3. In Section 4, the effectiveness and accuracy of the proposed method are proved by real-life experimental verification. Section 5 draws some conclusions.

2. Analysis of Auto-Transformer (AT) Double Track System Based on Multi-Conductor Transmission-Line (MTL) Theory

The cross section of standard 2×25 -kV AT railway system line is depicted in Figure 2, where the contact wire, carrier cable, two rails, protective wire, integrated earth wire and positive feeder in up traction network (down traction network) are marked as JW1(JW2), CW1(CW2), R1(R3), R2(R4), PW1(PW2), EW1(EW2) and FW1(FW2), respectively; and the earth is marked as E. Because each loop circuit is constituted by a transmission conductor and a return conductor while all the other conductors and the earth are return conductors, the standard railway system line in Figure 2 has 40 loop circuits. The numbers of all the loop circuits are shown in Table 1.

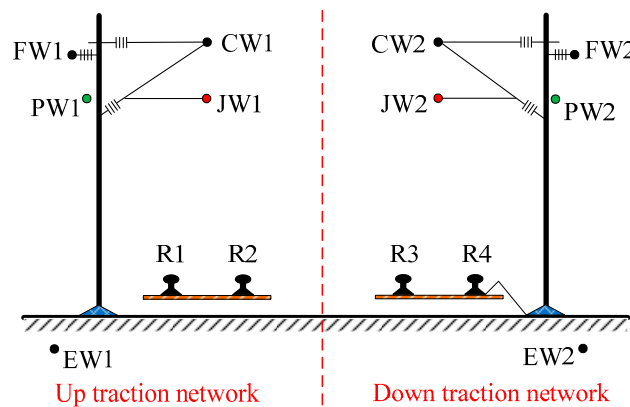


Figure 2. Typical cross section of auto-transformer (AT) double-track system.

Table 1. Loop circuit number of conductors in standard 2×25 kV auto-transformer (AT) railway system line.

Conductors	R1	R2	PW1	EW1	R3	R4	PW2	EW2	E	FW1	FW2
JW1	1	2	3	4	5	6	7	8	9	10	-
CW1	11	12	13	14	15	16	17	18	19	20	-
JW2	21	22	23	24	25	26	27	28	29	-	30
CW2	31	32	33	34	35	36	37	38	39	-	40

In the AT system, return conductors can be divided into magnetic field conversion return conductors and electric field return conductors. FW1, FW2 in Figure 2 belong to the former because they constitute loop circuits via the magnetic field conversion of the auto-transformer substation (ATS). R1, R2, PW1, EW1, R3, R4, PW2, EW2, E belong to the latter because they constitute loop circuits by connecting with each other through conductors/leakage conductance, or contacting the rail with the HST’s wheel.

The AT system is composed of two types of AT segments. One is the path between the traction substation (TSS) and the ATS. The other is the path between the adjacent ATs. For the two types of AT segments, the path at which load (expressed as HST here) is located is called the segment loop

circuit while the path at which the load is not located is called the long loop circuit. That is, when the load is located at the path between the TSS and the ATS, the path between the TSS and the ATS is the segment loop circuit while the other path is the long loop circuit. When the load is located at the path between the ATSSs, the path between the TSS and the ATS is the long loop circuit while the other path is the segment loop circuit.

Figure 3 depicts the currents of the AT system when assuming that the transmission conductors, electric field return conductors and magnetic field conversion return conductor are marked as T, N and F. In Figure 3, i_{T1} and i_{T2} are currents of T at the left and right sides of the load, respectively; i_{R1} and i_{R2} are currents of N at the left side and right side of load; i_{F1} is current of F at path of segment loop circuit; i' is load current; i_T , i_F and i_G are respectively total currents of T, F and N in the up and down traction network; u_T is potential to earth of positive bus-bar in the TSS; u_F is potential to earth of the negative bus-bar in the TSS. Both the distance between the TSS and ATS and the distance between adjacent ATSSs are assumed to be D . When the load is located at the path between the TSS and ATS, x is the distance between the load and TSS at the left side; when the load is located at the path between adjacent ATSSs, x is the distance between the load and ATS at the left side.

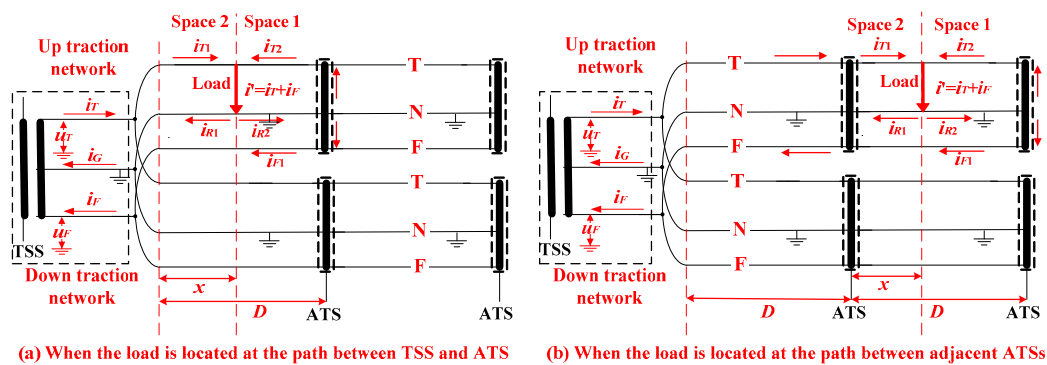


Figure 3. Currents of AT double-track system in a high-speed railway (HSR).

For the complete and accurate spatial magnetic field description of the AT system, obtaining complete and exact current distribution is the premise, and solving the precise traction network integrated impedance is an important aim. Thus, the deductions of current distribution and integrated impedance (marked as Z_0 here) implement the process of description. As for Z_0 , this is the integrated impedance of all the traction network loop circuits in parallel from the location of the traction substation to the location of the load or short-circuit point.

As the load is located at the path between the TSS and ATS in Figure 3a, unit length Z_0 is obtained by:

$$Z_0 = \frac{u_T + u_F}{(i_T + i_F)x} = \frac{u_T + u_F}{i'x} \quad (1)$$

As the load is located at the path between adjacent ATSSs in Figure 3b, unit length Z_0 is obtained by:

$$Z_0 = \frac{u_T + u_F}{(i_T + i_F)(D + x)} = \frac{u_T + u_F}{i'(D + x)} \quad (2)$$

In addition, Equation (3) shows the relation among u_T , u_F , i' , i_T , i_G , i_F [22].

$$\begin{cases} u_T = u_F \\ i' = i_T + i_F \\ i_T = i_G + i_F \end{cases} \quad (3)$$

In the segment loop circuit, return currents are borne by F and N. The relation among i_{R1} , i_{R2} and i_{F1} is often expressed as Equation (4) according to [22].

$$\begin{cases} i_{R1} = 2\left(\frac{D}{x} - 1\right) \cdot i_{F1} \\ i_{R2} = 2i_{F1} \end{cases} \quad (4)$$

According to Equation (4), when the load is running in the segment loop circuit, the distribution proportions of return currents in N and F will constantly change. At the beginning position of the segment loop circuit (i.e., $x = 0$ in Equation (4)), the return current is fully borne by N. At the terminal position of the segment loop circuit (i.e., $x = D$ in Equation (4)), the return current is fully borne by F. The current distribution and the segment loop circuit impedance are equal to that of the long loop circuit. So, to get the integrated impedance and current distribution of the whole AT double-track system, it is only necessary to obtain the deduction for the segment loop circuit. In addition, in terms of the Space 1 and the Space 2 seen in Figure 3, the deductions are separately made at first. Since the relation of i_{R1} , i_{F1} and the relation of i_{R2} , i_{F1} are different, the deduction processes of Space 1 and Space 2 are illustrated, as follows, separately.

3. Deduction Scheme Aimed at the Condition that the Load Exists in Up Traction Network or Down Traction Network

Because the parameters and the structure of the up and down traction networks are the same, the solution processes and results of current distribution and traction network integrated impedance are entirely identical. Thus, only the situation that the load exists in the up traction network is considered.

When the load is in the up traction network, the loop circuits of 1–20 are considered, as listed in Table 1. According to the relation between unit-length voltage drop and unit-length flux linkage of each loop circuit, when the source is a sinusoidal excitation, this can be obtained below.

$$\begin{bmatrix} \Delta u_1 \\ \Delta u_2 \\ \vdots \\ \Delta u_i \\ \vdots \\ \Delta u_{20} \end{bmatrix} = j\omega \begin{bmatrix} l_{1-1} & l_{1-2} & \cdots & l_{1-j} & \cdots & l_{1-20} \\ l_{2-1} & l_{2-2} & \cdots & l_{2-j} & \cdots & l_{2-20} \\ \vdots & \vdots & \ddots & \vdots & \ddots & \vdots \\ l_{i-1} & l_{i-2} & \cdots & l_{i-j} & \cdots & l_{i-20} \\ \vdots & \vdots & \ddots & \vdots & \ddots & \vdots \\ l_{20-1} & l_{20-2} & \cdots & l_{20-j} & \cdots & l_{20-20} \end{bmatrix} \begin{bmatrix} i_1 \\ i_2 \\ \vdots \\ i_j \\ \vdots \\ i_{20} \end{bmatrix} \quad (5)$$

where ω is angular velocity, Δu_i is voltage drop of loop circuit i , i_j is current of loop circuit j , l_{i-j} ($i = j$) is self-inductance of each loop circuit, and l_{i-j} ($i \neq j$) is mutual inductance between loop circuit i and loop circuit j ($i, j = 1, 2 \dots 20$).

3.1. Deduction for Space 1

The $i_{R2} = 2i_{F1}$ in Equation (4), i.e., the total currents of N are two times that of F. According to Table 1, considering that the total current of R1, R2, R3, R4, PW1, EW1, PW2, EW2, E is i_{R2} and the current of FW1 is i_{F1} , it is reasonable that $\sum_{i=1}^9 i_i + \sum_{j=11}^{19} i_j = i_{R2}$ and $i_{10} + i_{20} = i_{F1}$. In the synthesis of above relations, Equation (6) can be gained.

$$\sum_{i=1}^9 i_i + \sum_{j=11}^{19} i_j - 2i_{10} - 2i_{20} = 0 \quad (6)$$

Meanwhile, owing to the fact that the unit-length voltage drop between JW1 and FW1 is equal to the unit-length voltage drop between CW1 and FW1, this can be formulated as:

$$\Delta u_{10} = \Delta u_{20} \quad (7)$$

Then, by introducing Equations (6) and (7), the subtraction of Δu_{10} , Δu_{20} is performed and the current ratio of N and F is introduced in Equation (5). Equation (5) is transformed into Equation (8), where $a_i = l_{10-i} - l_{20-i}$ ($i = 1, 2, \dots, 20$) in the tenth row of inductance matrix.

$$\begin{bmatrix} \Delta u_1 \\ \vdots \\ \Delta u_9 \\ 0 \\ \Delta u_{11} \\ \vdots \\ \Delta u_{19} \\ 0 \end{bmatrix} = j\omega \begin{bmatrix} l_{1-1} & \cdots & l_{1-9} & l_{1-10} & l_{1-11} & \cdots & l_{1-19} & l_{1-20} \\ \vdots & \ddots & \vdots & \vdots & \vdots & \ddots & \vdots & \vdots \\ l_{9-1} & \cdots & l_{9-9} & l_{9-10} & l_{9-11} & \cdots & l_{9-19} & l_{9-20} \\ a_1 & \cdots & a_9 & a_{10} & a_{11} & \cdots & a_{19} & a_{20} \\ l_{11-1} & \cdots & l_{11-9} & l_{11-10} & l_{11-11} & \cdots & l_{11-19} & l_{11-20} \\ \vdots & \ddots & \vdots & \vdots & \vdots & \ddots & \vdots & \vdots \\ l_{19-1} & \cdots & l_{19-9} & l_{19-10} & l_{19-11} & \cdots & l_{19-19} & l_{19-20} \\ 1 & \cdots & 1 & -2 & 1 & \cdots & 1 & -2 \end{bmatrix} \begin{bmatrix} i_1 \\ \vdots \\ i_9 \\ i_{10} \\ i_{11} \\ \vdots \\ i_{19} \\ i_{20} \end{bmatrix} \tag{8}$$

Assuming that the total current of transmission conductors or return conductors is i_0 and the current distribution coefficient of each loop circuit of Space 1 is k_i ($i=1, 2 \dots 20$), $i_i = k_i i_0$ is gained. $\Delta u_1, \Delta u_2 \dots \Delta u_9, \Delta u_{11}, \Delta u_{12} \dots \Delta u_{19}$ are the unit-length potential difference between T and N and they can be seen as equal to each other. In view of this, $\Delta u_1 = \dots = \Delta u_9 = \Delta u_{11} = \dots = \Delta u_{19} = c_1$ (c_1 is arbitrary constant) is set. Then, focusing on Equation (8), by performing an inverse matrix transformation and introducing $i_i = k_i i_0$ and $\Delta u_1 = \dots = \Delta u_9 = \Delta u_{11} = \dots = \Delta u_{19} = c_1$, Equation (8) is transformed into Equation (9).

$$\begin{bmatrix} k_1 i_0 \\ \vdots \\ k_9 i_0 \\ k_{10} i_0 \\ k_{11} i_0 \\ \vdots \\ k_{19} i_0 \\ k_{20} i_0 \end{bmatrix} = \frac{1}{j\omega} \begin{bmatrix} l_{1-1} & \cdots & l_{1-9} & l_{1-10} & l_{1-11} & \cdots & l_{1-19} & l_{1-20} \\ \vdots & \ddots & \vdots & \vdots & \vdots & \ddots & \vdots & \vdots \\ l_{9-1} & \cdots & l_{9-9} & l_{9-10} & l_{9-11} & \cdots & l_{9-19} & l_{9-20} \\ a_1 & \cdots & a_9 & a_{10} & a_{11} & \cdots & a_{19} & a_{20} \\ l_{11-1} & \cdots & l_{11-9} & l_{11-10} & l_{11-11} & \cdots & l_{11-19} & l_{11-20} \\ \vdots & \ddots & \vdots & \vdots & \vdots & \ddots & \vdots & \vdots \\ l_{19-1} & \cdots & l_{19-9} & l_{19-10} & l_{19-11} & \cdots & l_{19-19} & l_{19-20} \\ 1 & \cdots & 1 & -2 & 1 & \cdots & 1 & -2 \end{bmatrix}^{-1} \begin{bmatrix} c_1 \\ \vdots \\ c_1 \\ 0 \\ c_1 \\ \vdots \\ c_1 \\ 0 \end{bmatrix} \tag{9}$$

For Equation (9), after calculating the coefficients of the inductance matrix and eliminating i_0 in the first column, the values of $k_1, k_2 \dots k_{20}$, are deduced. Subsequently, by introducing $i_i = k_i i_0$ into Equation (5), it can be found that,

$$\begin{bmatrix} \Delta u_1 \\ \Delta u_2 \\ \vdots \\ \Delta u_i \\ \vdots \\ \Delta u_{20} \end{bmatrix} = \begin{bmatrix} k_1 l_{1-1} & k_2 l_{1-2} & \cdots & k_j l_{1-j} & \cdots & k_{20} l_{1-20} \\ k_1 l_{2-1} & k_2 l_{2-2} & \cdots & k_j l_{2-j} & \cdots & k_{20} l_{2-20} \\ \vdots & \vdots & \ddots & \vdots & \ddots & \vdots \\ k_1 l_{i-1} & k_2 l_{i-2} & \cdots & k_j l_{i-j} & \cdots & k_{20} l_{i-20} \\ \vdots & \vdots & \ddots & \vdots & \ddots & \vdots \\ k_1 l_{20-1} & k_2 l_{20-2} & \cdots & k_j l_{20-j} & \cdots & k_{20} l_{20-20} \end{bmatrix} \begin{bmatrix} j\omega i_0 \\ j\omega i_0 \\ \vdots \\ j\omega i_0 \\ \vdots \\ j\omega i_0 \end{bmatrix} \tag{10}$$

By substituting the deduced values of $k_1, k_2 \dots k_{20}$ into Equation (10), $\Delta u_1, \Delta u_2 \dots \Delta u_{20}$ are acquired. However, because the i_0 of Equation (10) is still unknown, the deduced $\Delta u_1, \Delta u_2 \dots \Delta u_{20}$ are not values, but are mathematical expressions of i_0 . Meanwhile, due to $\Delta u_1 = \dots = \Delta u_9 = \Delta u_{11} = \dots = \Delta u_{19}$ and $\Delta u_{10} = \Delta u_{20}$, it can be understandable that the obtained expressions of $\Delta u_1, \Delta u_2 \dots \Delta u_9, \Delta u_{11} \dots \Delta u_{19}$ are equal while the obtained expressions of $\Delta u_{10}, \Delta u_{20}$ are equal. On this basis, we can assume that $\Delta u_1 = \dots = \Delta u_9 = \Delta u_{11} = \dots = \Delta u_{19} = f_1(i_0)$ and $\Delta u_{10} = \Delta u_{20} = g_1(i_0)$. Unit-length electric field return

impedance of Space 1 (marked as Z_1) is calculated by $Z_1 = f_1(i_0)/i_0$. Unit-length magnetic field conversion return impedance of Space 1 (marked as Z_2) is calculated by $Z_2 = g_1(i_0)/i_0$.

The traction network loop circuits can be divided into the overhead loop circuit and earth return loop circuit. The former is composed only of conductors while the latter is composed of the conductor and the earth. For the two types of loop circuits, the calculation formulas of the inductance matrix coefficients in Equation (5) are different. As for the overhead loop circuit, the inductance coefficients are calculated by using the fundamental formulas of loop circuit inductance [25,26]. As for the earth return loop circuit, considering that the earth is a part of the loop circuit, the inductance coefficients are calculated with the Carson formula [27,28].

3.2. Deduction for Space 2

The $i_{R1} = 2\left(\frac{D}{x} - 1\right) \cdot i_{F1}$ in Equation (4) is introduced.

At first, combining $i_{R1} = 2\left(\frac{D}{x} - 1\right) \cdot i_{F1}$ and Table 1, $\sum_{i=1}^9 i_i + \sum_{j=11}^{19} i_j = i_{R1}$, $i_{10} + i_{20} = i_{F1}$ and Equation (11) are given.

$$\sum_{i=1}^9 i_i + \sum_{j=11}^{19} i_j + 2\left(1 - \frac{D}{x}\right)(i_{10} + i_{20}) = 0 \tag{11}$$

Meanwhile, being similar to the unit-length voltage drop relationship in Space 1,

$$\Delta u_{10} = \Delta u_{20} \tag{12}$$

By introducing Equations (11) and (12), Equation (5) is changed into Equation (13).

$$\begin{bmatrix} \Delta u_1 \\ \vdots \\ \Delta u_9 \\ 0 \\ \Delta u_{11} \\ \vdots \\ \Delta u_{19} \\ 0 \end{bmatrix} = j\omega \begin{bmatrix} l_{1-1} & \cdots & l_{1-9} & l_{1-10} & l_{1-11} & \cdots & l_{1-19} & l_{1-20} \\ \vdots & \ddots & \vdots & \vdots & \vdots & \ddots & \vdots & \vdots \\ l_{9-1} & \cdots & l_{9-9} & l_{9-10} & l_{9-11} & \cdots & l_{9-19} & l_{9-20} \\ a_1 & \cdots & a_9 & a_{10} & a_{11} & \cdots & a_{19} & a_{20} \\ l_{11-1} & \cdots & l_{11-9} & l_{11-10} & l_{11-11} & \cdots & l_{11-19} & l_{11-20} \\ \vdots & \ddots & \vdots & \vdots & \vdots & \ddots & \vdots & \vdots \\ l_{19-1} & \cdots & l_{19-9} & l_{19-10} & l_{19-11} & \cdots & l_{19-19} & l_{19-20} \\ 1 & \cdots & 1 & 2\left(1 - \frac{D}{x}\right) & 1 & \cdots & 1 & 2\left(1 - \frac{D}{x}\right) \end{bmatrix} \begin{bmatrix} i_1 \\ \vdots \\ i_9 \\ i_{10} \\ i_{11} \\ \vdots \\ i_{19} \\ i_{20} \end{bmatrix} \tag{13}$$

where $a_i = l_{10-i} - l_{20-i}$ ($i = 1, 2 \dots 20$) in the tenth row of inductance matrix.

As for Space 2, given that total current of transmission conductors or return conductors is i_0' and current distribution coefficient of each loop circuit is k_i' ($i = 1, 2 \dots 20$), it is obvious that $i_i = k_i' \cdot i_0'$ ($i = 1, 2 \dots 20$). Then, being similar to Space 1, by performing the inverse matrix transformation, introducing $i_i = k_i' \cdot i_0'$ ($i = 1, 2 \dots 20$) and setting $\Delta u_1, \Delta u_2 \dots \Delta u_9, \Delta u_{11} \dots \Delta u_{19}$ to an arbitrary equal constant of c_2 in Equation (13), Equation (14) is then obtained.

$$\begin{bmatrix} k_1' i_0' \\ \vdots \\ k_9' i_0' \\ k_{10}' i_0' \\ k_{11}' i_0' \\ \vdots \\ k_{19}' i_0' \\ k_{20}' i_0' \end{bmatrix} = \frac{1}{j\omega} \begin{bmatrix} l_{1-1} & \cdots & l_{1-9} & l_{1-10} & l_{1-11} & \cdots & l_{1-19} & l_{1-20} \\ \vdots & \ddots & \vdots & \vdots & \vdots & \ddots & \vdots & \vdots \\ l_{9-1} & \cdots & l_{9-9} & l_{9-10} & l_{9-11} & \cdots & l_{9-19} & l_{9-20} \\ a_1 & \cdots & a_9 & a_{10} & a_{11} & \cdots & a_{19} & a_{20} \\ l_{11-1} & \cdots & l_{11-9} & l_{11-10} & l_{11-11} & \cdots & l_{11-19} & l_{11-20} \\ \vdots & \ddots & \vdots & \vdots & \vdots & \ddots & \vdots & \vdots \\ l_{19-1} & \cdots & l_{19-9} & l_{19-10} & l_{19-11} & \cdots & l_{19-19} & l_{19-20} \\ 1 & \cdots & 1 & 2\left(1 - \frac{D}{x}\right) & 1 & \cdots & 1 & 2\left(1 - \frac{D}{x}\right) \end{bmatrix}^{-1} \begin{bmatrix} c_2 \\ \vdots \\ c_2 \\ 0 \\ c_2 \\ \vdots \\ c_2 \\ 0 \end{bmatrix} \tag{14}$$

In Equation (14), after calculating the self and mutual inductance of the loop circuit matrix and eliminating i_0' in the first column, the values of $k_1', k_2' \dots k_{20}'$ are obtained.

$$\begin{bmatrix} \Delta u_1 \\ \Delta u_2 \\ \vdots \\ \Delta u_i \\ \vdots \\ \Delta u_{20} \end{bmatrix} = \begin{bmatrix} k_1' l_{1-1} & k_2' l_{1-2} & \dots & k_j' l_{1-j} & \dots & k_{20}' l_{1-20} \\ k_1' l_{2-1} & k_2' l_{2-2} & \dots & k_j' l_{2-j} & \dots & k_{20}' l_{2-20} \\ \vdots & \vdots & \ddots & \vdots & \ddots & \vdots \\ k_1' l_{i-1} & k_2' l_{i-2} & \dots & k_j' l_{i-j} & \dots & k_{20}' l_{i-20} \\ \vdots & \vdots & \ddots & \vdots & \ddots & \vdots \\ k_1' l_{20-1} & k_2' l_{20-2} & \dots & k_j' l_{20-j} & \dots & k_{20}' l_{20-20} \end{bmatrix} \begin{bmatrix} j\omega i_0' \\ j\omega i_0' \\ \vdots \\ j\omega i_0' \\ \vdots \\ j\omega i_0' \end{bmatrix} \tag{15}$$

Subsequently, by substituting the obtained values of $k_1', k_2' \dots k_{20}'$ into Equation (15), $\Delta u_1, \Delta u_2 \dots \Delta u_{20}$ are deduced. Similarly, with Space 1, for the reason that the deduced $\Delta u_1, \Delta u_2 \dots \Delta u_{20}$ are mathematical expressions of i_0' and $\Delta u_1 = \dots = \Delta u_9 = \Delta u_{11} = \dots = \Delta u_{19}$ while $\Delta u_{10} = \Delta u_{20}$, we assume that $\Delta u_1 = \dots = \Delta u_9 = \Delta u_{11} = \dots = \Delta u_{19} = f_2(i_0')$ and $\Delta u_{10} = \Delta u_{20} = g_2(i_0')$. The unit-length electric field return impedance of Space 2 (marked as Z_1') is calculated by $Z_1' = f_2(i_0')/i_0'$. The unit-length magnetic field conversion return impedance of Space 2 (marked as Z_2') is calculated by $Z_2' = g_2(i_0')/i_0'$.

However, the result of $i_{R1} = 2\left(1 - \frac{D}{x}\right) \cdot i_{F1}$ in Equation (4) is valid only when the spatial position between T and N is symmetrical with the spatial position between N and F and the self-impedance of T is equal to the self-impedance of F. The aforementioned deduced values of $k_1', k_2' \dots k_{20}', Z_1'$ and Z_2' are inaccurate and they can only be regarded as initial results.

According to the transformer ratio transformer of AT in Space 2, the voltage drop between T and N, i.e., u in Figure 4 should be equal to the voltage drop between N and F, i.e., u' in Figure 4.

$$u = u' \tag{16}$$

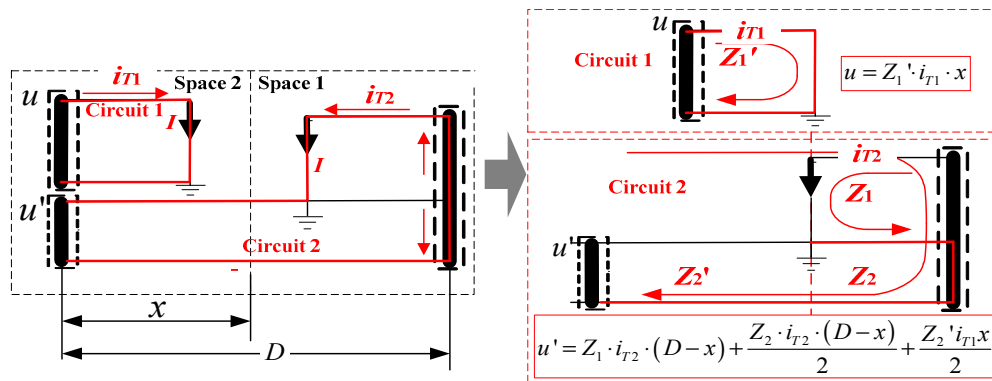


Figure 4. Segment loop circuit network separated by load.

For the $\begin{cases} u = Z_1' \cdot i_{T1} \cdot x \\ u' = Z_1 \cdot i_{T2} \cdot (D-x) + \frac{Z_2 \cdot i_{T2} \cdot (D-x)}{2} + \frac{Z_2' \cdot i_{T1} \cdot x}{2} \end{cases}$ in Figure 4, the values of Z_1 and Z_2 have been obtained after introducing the $i_{R2} = 2i_{F1}$ of Equation (4) into the inductance matrix of Space 1; the values of Z_1' and Z_2' have been obtained after introducing the $i_{R1} = 2\left(\frac{D}{x} - 1\right) \cdot i_{F1}$ of Equation (4) into the inductance matrix of Space 2. According to Equation (4) and the circuit of the AT system, the relation of i_{T1}, i_{T2}, i_{F1} satisfies

$$\begin{cases} i_{T1} = \left(\frac{2D}{x} - 1\right) \cdot i_{F1} \\ i_{T2} = i_{F1} \end{cases} \tag{17}$$

By introducing Equation (17) into $\begin{cases} u = Z'_1 \cdot i_{T1} \cdot x \\ u' = Z_1 \cdot i_{T2} \cdot (D - x) + \frac{Z_2 \cdot i_{T2} \cdot (D - x)}{2} + \frac{Z'_2 \cdot i_{T1} \cdot x}{2} \end{cases}$, determining $x = x_0$ (according to the location of load) and setting i_{F1} as an arbitrary constant of c , it can be found that

$$\begin{cases} u = (2D - x_0) \cdot c \cdot Z'_1 \\ u' = c \cdot Z_1 \cdot (D - x_0) + \frac{Z_2 \cdot c \cdot (D - x_0)}{2} + \frac{Z'_2 \cdot (2D - x_0) \cdot c}{2} \end{cases} \quad (18)$$

In Equation (18), u and u' are always unequal for the reason that the granted results of $i_{R1} = 2\left(1 - \frac{D}{x}\right) \cdot i_{F1}$ are valid only as an approximation. In order to obtain exact results, an iterative calculation method aimed at satisfying the constraint condition of Equation (16) is proposed, as demonstrated in Figure 5.

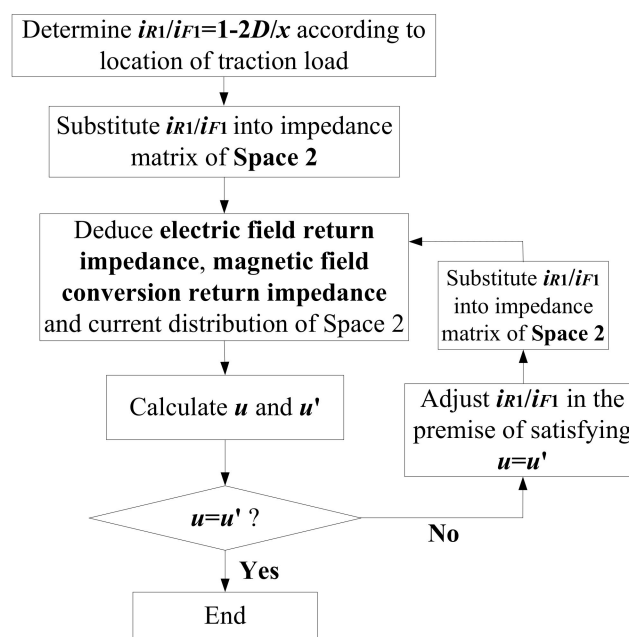


Figure 5. Flowchart of the iterative calculation aimed at satisfying the constraint condition in Equation (16).

In the beginning, the i_{R1}/i_{F1} is adjusted to deduce new values of $k_1', k_2' \dots k_{20}', Z_1'$ and Z_2' . On this basis, new u and u' are obtained after introducing new i_{T1}/i_{T2} and new values of Z_1' and Z_2' into $\begin{cases} u = Z'_1 \cdot i_{T1} \cdot x_0 \\ u' = Z_1 \cdot i_{T2} \cdot (D - x_0) + \frac{Z_2 \cdot i_{T2} \cdot (D - x_0)}{2} + \frac{Z'_2 \cdot i_{T1} \cdot x_0}{2} \end{cases}$. If $u = u'$ is still not satisfied, i_{R1}/i_{F1} continues to be adjusted and corresponding calculation is repeated again. Only when u nearly approximates to u' are the deduced values of $k_1', k_2' \dots k_{20}', Z_1'$ and Z_2' considered as final and accurate results for Space 2.

When the final and accurate values of Z_1' and Z_2' are determined, the impedance of circuit 1 in Figure 4 (marked as Z_a) and the impedance of circuit 2 in Figure 4 (marked as Z_b) are, respectively, calculated by Equations (19) and (20).

$$Z_a = Z'_1 \cdot x_0 \quad (19)$$

$$Z_b = Z_1 \cdot (D - x_0) + \frac{Z_2 \cdot (D - x_0)}{2} + \frac{Z'_2 \cdot x_0}{2} \quad (20)$$

The impedance of the segment loop circuit (marked as Z_A) is the parallel impedance of Z_a and Z_b , namely,

$$Z_A = Z_a // Z_b = \frac{2Z_1Z_1'x_0(D-x_0) + Z_1'Z_2x_0(D-x_0) + Z_1'Z_2'x_0^2}{2Z_1'x_0 + 2Z_1(D-x_0) + Z_2(D-x_0) + Z_2'x_0} \tag{21}$$

When the load is located at the path between the TSS and ATS, the unit-length traction network impedance (marked as Z) is obtained by utilizing Equation (22).

$$Z = \frac{Z_A}{x_0} = \frac{2Z_1Z_1'x_0(D-x_0) + Z_1'Z_2x_0(D-x_0) + Z_1'Z_2'x_0^2}{2Z_1'x_0^2 + 2Z_1x_0(D-x_0) + Z_2x_0(D-x_0) + Z_2'x_0^2} \tag{22}$$

When the load is located at the path between adjacent ATSS, the traction network impedance is composed of Z_A and impedance of the long loop circuit (marked as Z_B). As mentioned in Section 2, when $x = D$, the return current is fully borne by F. The current distribution and impedance of the segment loop circuit are equal to that of the long loop circuit. Therefore, after substituting $x = D$ for $x = x_0$ in Equation (21), Z_B is deduced as

$$Z_B = \frac{Z_1'Z_2'D}{2Z_1' + Z_2'} \tag{23}$$

So, when the load is located at the path between adjacent ATSS, Z is obtained by utilizing Equation (24).

$$Z = \frac{Z_A + Z_B}{x_0(D+x_0)} = \frac{2Z_1Z_1'x_0(D-x_0) + Z_1'Z_2x_0(D-x_0) + Z_1'Z_2'x_0^2}{2Z_1'(Dx_0^2+x_0^3) + 2Z_1x_0(D^2-x_0^2) + Z_2x_0(D^2-x_0^2) + Z_2'(Dx_0^2+x_0^3)} + \frac{Z_1'Z_2'D}{(2Z_1' + Z_2')(Dx_0+x_0^2)} \tag{24}$$

4. Experimental Verification

To prove the effectiveness of proposed method effectively and accurately, two short-circuit experiments at different Chinese HSR lines were performed. The first experiment was carried out in the feeding arm of Jiangyou substation on the Chengdu–Chongqing HSR line on 11 October 2015. The second short-circuit experiment was carried out in the feeding arm of Qinglinkou substation on the Xian–Chengdu HSR line on 12 July 2017. The cross section and parameters of traction network conductors in the experiments are shown in Figure 2 and Table 2. The numbers of all the loop circuits in the experiments are listed in Table 1. In the two short-circuit experiments, flexible copper stranded conductor was used to short-circuit the rail and the catenary.

Table 2. Parameters of all the conductor wires in the HSR line from Chengdu to Chongqing.

Cable and Its Horizontal and Vertical Coordination (cm)	Type	DC Resistance (Ω/km)	Calculated Radius (cm)
JW1 (0, 530), JW2 (460, 530)	CTS-150	0.15967	0.72
CW1 (0, 690), CW2 (460, 690)	JTMH-120	0.242	0.7
R1 (−71.75, 0), R2 (71.75, 0), R3 (388.25, 0), R4 (531.75, 0)	60kg	0.135	1.279
PW1 (−340, 690), PW2 (800, 690)	LBJLJ-120/20	0.2382	0.763
EW1 (−400, −246), EW2 (860, −246)	DH-70	0.312	0.437
FW1 (−410, 680), FW2 (870, 680)	LBGLJ-240/30	0.1181	1.08

Figures 6 and 7 depict the circuit diagram and scene diagram of two short-circuit experiments. According to Figure 6, whether for the first short-circuit experiment or the second short-circuit experiment, switches A1, A2, A4, A6, A13, A14, A17 and A18 are closed and the other switches are opened to simulate the standard $2 \times 25\text{-kV}$ AT double track power supply mode. The effective values of all the measured currents are shown in Table 3. In addition, the low-voltage side bus voltages of the traction substation

and the total currents of the transmission conductors are, respectively, collected at the secondary side of the traction transformer and current transformer in the position of switch A1. According to the collection results, the measured integrated impedance can be obtained.

Based on the proposed deduction method, the current distribution coefficients of conductors in the short-circuit experiments are calculated in Table 4, after the initial current distribution is continuously adjusted to satisfy the constraint condition of real circuit voltages as much as possible. Compared with existing analysis results of current distribution in the traction network ([21,29]), the deduced results in Table 4 are reasonable. Furthermore, according to Table 4, the deduced current distribution coefficients of T, N and F are 0.6235, 0.2138 and 0.3765, respectively. According to Table 3, the measured current distribution coefficients of T, N and F in the first short-circuit experiment are 0.6304 (I_T/I), 0.1985 (I_G/I) and 0.3673 (I_F/I), respectively, and the measured current distribution coefficients of T, N and F in the second short-circuit experiment are 0.6233 (I_T/I), 0.2180 (I_G/I) and 0.4055 (I_F/I), respectively. The comparison between the measured current distribution coefficients and the deduced current distribution coefficients is demonstrated in Figure 8. Obviously, the deduced results are very close to the measured results.

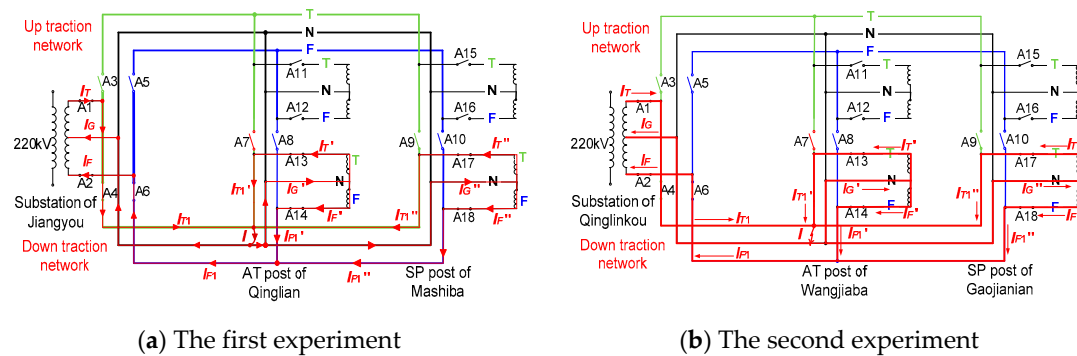


Figure 6. Circuit diagrams of the two short-circuit experiments.

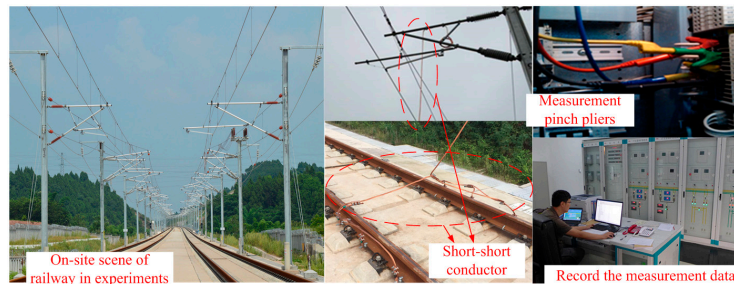


Figure 7. Scene diagrams of the short-circuit experiments.

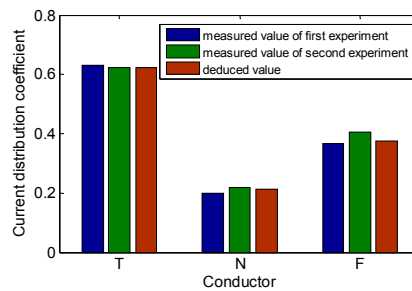


Figure 8. Comparison between measurement results and results of deduction for the current distribution.

Table 3. Measurement record of currents of the short-circuit experiments.

First Short-Circuit Experiment				Second Short-Circuit Experiment			
Current	Effective value (A)	Current	Effective Value (A)	Current	Effective Value (A)	Current	Effective Value (A)
I_T	2755	I_G	867.48	I_T	2224.1	I_G	777.77
I_F	1605	I_{T1}	2755.43	I_F	1447.0	I_{T1}	2223.7
I_{F1}	1605.27	I_{T1}'	1395.07	I_{F1}	1446.68	I_{T1}'	1148.04
I_{F1}'	1395.48	I_T'	1395.73	I_{F1}'	1148.02	I_T'	1148.1
I_G'	2790.37	I_F'	1395.89	I_G'	2296.05	I_F'	1148.06
I_{T1}''	219.69	I_{F1}''	219.40	I_{T1}''	196.29	I_{F1}''	196.24
I_T''	219.89	I_G''	439.41	I_T''	196.34	I_G''	392.56
I_F''	219.71	I	4370.19	I_F''	196.32	I	3568

Table 4. Derived current distribution coefficients aimed at the short-circuit experiments.

Cable	Related Loop Circuits	Deduced Coefficient
JW	1, 2 ... 10	0.3296
CW	10, 11 ... 20	0.2939
R(R1 + R2 + R3 + R4)	1, 2, 5, 6, 11, 12, 15, 16	0.1315
PW(PW1 + PW2)	3, 7, 13, 17	0.0518
EW(EW1 + EW2)	4, 8, 14, 18	0.0305
FW(FW1 + FW2)	10, 20	0.3765
E	9, 19	0.0332

Furthermore, according to measurement records, the unit-length amplitude and phase angle of integrated impedance were $0.3446 \Omega/\text{km}$ and 73.54° in the first short-circuit experiment; and the unit-length amplitude and phase angle of integrated impedance were $0.3614 \Omega/\text{km}$ and 71.63° in the second short-circuit experiment. Relatively, the derived unit-length amplitude and phase angle of integrated impedance were $0.3576 \Omega/\text{km}$ and 69.95° , considering the iterative solution of approaching the constraint condition. Figure 9 depicts the comparison of the above results by using histograms. It can be demonstrated that both the measurement results of the two short-circuit experiments are almost identical to the derived results.

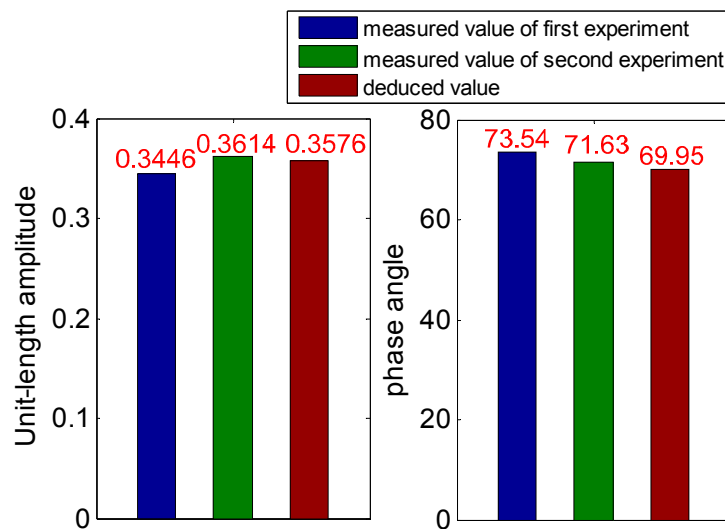


Figure 9. Comparison between measurement results and results of deduction for the integrated impedance.

5. Conclusions

This paper is concerned with the AT system in HSR and proposes a spatial magnetic field description method, combined with the ideas of a multi-conductor loop circuit and iteration. This method cannot only directly reflect the complete current distribution of a traction network, but also deduce the exact traction network integrated impedance.

First, due to the limitations of the existing approach, the hypothesis that the earth is the reference conductor of a structuring loop circuit matrix is cancelled. To satisfy the condition of complete and accurate spatial magnetic field description, all the real traction network loop circuits and their self and mutual inductance influences are considered in order to list the loop circuit matrix of the AT system.

Next, considering the actual electrical structure of the AT system, different description processes are divided, respectively, for the right side of the load (Space 1) and the left side of the load (Space 2). Considering that the two types of return conductors have different potential differences with the transmission conductor in the AT system, certain current ratios deduced in existing studies are introduced. For Space 1, after directly introducing the current ratio into the loop circuit matrix and performing some matrix transformations on this basis, the complete current distribution and the impedance of the traction network can be obtained. For Space 2, after directly introducing the current ratio into the loop circuit matrix and performing some matrix transformations on this basis, the deduced results are actually inaccurate, for the reason that the introduced current ratio of Space 2 is approximate. Therefore, an iterative scheme is adopted for the deduction of Space 2. According to the transformer ratio of the AT substation, a constraint condition of circuit voltages is determined. By approximately searching and adjusting the current ratio to satisfy the constraint condition of circuit voltages, accurate current distribution and traction network integrated impedance are finally obtained.

Finally, experimental verification was undertaken. The results demonstrate that the presented method has the capability to depict the exact current distribution and traction network integrated impedance of an AT system.

Further investigations on the improvement of the spatial magnetic field description method of an AT system are necessary. For example, it is feasible to obtain the exact rail potential distribution if the leakage conductance between rail and earth is considered in the establishment of the loop circuit matrix. Also, some engineering applications of the description method, such as testing software development, can be further studied.

Author Contributions: Conceptualization, Y.D. and K.H.; Methodology, Y.D.; Software, D.S.; Validation, Y.D., K.H. and Z.L.; Formal Analysis, Y.D.; Investigation, Y.D.; Resources, Z.L.; Data Curation, D.S.; Writing-Original Draft Preparation, K.H.; Writing-Review & Editing, Z.L.; Visualization, Y.D.; Supervision, Z.L.; Project Administration, Y.D.; Funding Acquisition, Y.D.

Funding: This research was funded by National Nature Science Foundation of China [U1434203, U1734202], Sichuan Province Youth Science and Technology Innovation Team [2016TD0012] and Research Project of China Railway Eryuan Engineering Group Co. Ltd. [KYY2017025(17-18)]

Acknowledgments: This work is supported by the National Nature Science Foundation of China (U1434203, U1734202), Sichuan Province Youth Science and Technology Innovation Team (2016TD0012), and Research Project of China Railway Eryuan Engineering Group Co. Ltd. (KYY2017025(17-18)).

Conflicts of Interest: The authors declare no conflict of interest.

References

1. Wu, M.L. Uniform chain circuit model for traction networks of electric railways. *Proc. CSEE* **2010**, *30*, 52–58.
2. Wang, Q.; Liu, Z.G.; Bai, W.L.; Tu, F.R. Research on the simulation model of traction power supply system based on PSCAD/EMTDC. *Power Syst. Protect. Control* **2009**, *37*, 35–45.
3. Brenna, M.; Foadelli, F.; Zaninelli, D. Electromagnetic model of high speed railway lines for power quality studies. *IEEE Trans. Power Syst.* **2010**, *25*, 1301–1308. [[CrossRef](#)]

4. Dolara, A.; Gualdoni, M.; Leva, S. Impact of high-voltage primary supply lines in the 2×25 kv 50 Hz railway system on the equivalent impedance at pantograph terminals. *IEEE Trans. Power Deliv.* **2012**, *27*, 164–175. [[CrossRef](#)]
5. Cella, R.; Giangaspero, G.; Mariscotti, A.; Montepagano, A.; Pozzobon, P.; Ruscelli, M.; Vanti, M. Measurement of AT electric railway system currents at power-supply frequency and validation of a multiconductor transmission-line model. *IEEE Trans. Power Deliv.* **2006**, *21*, 1721–1726. [[CrossRef](#)]
6. Song, W.S.; Jiao, S.L.; Li, Y.W.; Wang, J.; Huang, J. High-frequency harmonic resonance suppression in high-speed railway through single-phase traction converter with LCL filter. *IEEE Trans. Transp. Electr.* **2016**, *2*, 347–356. [[CrossRef](#)]
7. Guo, X.X.; Li, Q.Z.; Xie, S.F.; Yi, D.; Wang, H.; Song, J.W. Electrical characteristic of cable traction network for electrified railway. *Electr. Power Autom. Equip.* **2015**, *35*, 132–137.
8. D'Addio, G.; Fracchia, M.; Mariscotti, A.; Pozzobon, P. Sensitivity analysis of railway line impedance to variations of electrical and geometrical parameters. In Proceedings of the World Congress on Railway Research WCRR, Tokyo, Japan, 19–23 October 1999; Volume 19, pp. 19–23.
9. Mariscotti, A.; Pozzobon, P.; Vanti, M. Distribution of the traction return current in AT electric railway systems. *IEEE Trans. Power Deliv.* **2005**, *20*, 2119–2128. [[CrossRef](#)]
10. Zhang, G.N.; Liu, Z.G.; Yao, S.; Liao, Y.; Xiang, C. Suppression of low-frequency oscillation in traction network of high-speed railway based on auto-disturbance rejection control. *IEEE Trans. Transp. Electr.* **2016**, *2*, 244–255. [[CrossRef](#)]
11. Chou, C.J.; Hsiao, Y.T.; Wang, J.L.; Hwang, Y.T. Distribution of earth leakage currents in railway systems with drain auto-transformers. *IEEE Trans. Power Deliv.* **2001**, *16*, 271–275. [[CrossRef](#)]
12. Rienzo, L.D.; Zhang, Z.C.; Pignari, S.A. Boundary-element computation of per-unit-length series parameters of railway lines. *IEEE Trans. Electromagn. Compat.* **2009**, *51*, 825–832. [[CrossRef](#)]
13. Lin, G.H.; Zhang, Y.R.; Zhi, Y.J. Effects of pantograph arcing on railway systems with auto transformers. *J. Electromagn. Waves Appl.* **2013**, *27*, 1686–1693. [[CrossRef](#)]
14. Huang, K.; Liu, Z.G.; Zhu, F.; Zheng, Z.S.; Cheng, Y. Evaluation scheme for EMI of train body voltage fluctuation on the BCU speed sensor measurement. *IEEE Trans. Instrum. Meas.* **2017**, *66*, 1046–1057. [[CrossRef](#)]
15. Wang, Y.; Liu, Z.G.; Mu, X.Q.; Huang, K.; Wang, H.R.; Gao, S.B. An extended Habedank's equation-based EMTP model of pantograph arcing considering pantograph-catenary interactions and train speeds. *IEEE Trans. Power Deliv.* **2016**, *31*, 1186–1194. [[CrossRef](#)]
16. Xiang, N.W.; Chen, W.J.; Bian, K.; Li, C.R.; Chen, J.H.; Gu, S.Q.; Shen, H.B. The electromagnetic transient model for high-speed railway viaducts struck by lightning based on the decoupling method. *IEEE Trans. Electromagn. Compat.* **2016**, *58*, 1541–1548. [[CrossRef](#)]
17. Zhang, G.N.; Liu, Z.G.; Guo, X.X.; Gao, S.B. Modeling and analysis of traction network of high-speed railway tunnel/viaduct sections. *J. China Railw. Soc.* **2015**, *37*, 16–24.
18. Wang, Y.; Liu, Z.G.; Mu, X.Q.; Song, X.C.; Huang, K.; Deng, C.Y. Research on electromagnetic transient process in articulated splitphase insulator of high-speed railway considering viaduct's electrical coupling. *Int. Trans. Electr. Energy Syst.* **2017**, *27*, 1–19. [[CrossRef](#)]
19. Cheng, Y.; Liu, Z.G.; Huang, K. Transient analysis of electric arc burning at insulated rail joints in high-speed railway stations based on state-space modeling. *IEEE Trans. Transp. Electr.* **2017**, *3*, 750–761. [[CrossRef](#)]
20. Cheng, Y.; Liu, Z.G.; Huang, K.; Zhou, H.Y. Modeling analysis of electric multiple units passing insulated rail joints in high-speed railway station. In Proceedings of the 2017 Asia-Pacific IEEE International Transportation Electrification Conference, Harbin, China, 7–10 August 2017; pp. 1–6.
21. Zhang, J.Q.; Wu, M.L. Calculation method of OCS ampacity for electric railway. *J. China Railw. Soc.* **2015**, *37*, 40–45.
22. Li, Q.Z.; He, J.M. *Analysis of Traction Power Supply System*; Southwest Jiaotong University Press: Chengdu, China, 2012.
23. Deng, Y.C.; Liu, Z.G.; Wang, Y.; Huang, K. Study on application of all-parallel DN power supply mode on montanic electrified railway. In Proceedings of the 2015 International Conference on Electrical and Information Technologies for Rail Transportation, Zhuzhou, China, 17–19 October 2015.
24. Brenna, M.; Foiadelli, F. Sensitivity analysis of the constructive parameters for the 2×25 -kV high-speed railway lines planning. *IEEE Trans. Power Deliv.* **2010**, *25*, 1923–1931. [[CrossRef](#)]
25. Matick, R.E. *Transmission Lines for Digital and Communication Networks*; McGraw-Hill Press: New York, NY, USA, 1969.

26. Harrington, R.F.; Wei, C. Losses in multiconductor transmission lines in multilayered dielectric media. *IEEE Trans. Microw. Theory Tech.* **1984**, *32*, 705–710. [[CrossRef](#)]
27. Carson, J.R. Wave propagation in overhead wires with ground return. *Bell Syst. Tech. J.* **1926**, *5*, 339–359. [[CrossRef](#)]
28. Perz, M.C.; Raghuvver, M.R. Generalized derivation of fields, and impedance correction factors of lossy transmission lines. Part 1. Lossy conductors above lossy ground. *IEEE Trans. Power Appar. Syst.* **1974**, *93*, 1832–1841. [[CrossRef](#)]
29. Research Report of China Academy of Railway Sciences. *Study on the Return Index of High Speed Railway Integrated Grounding System*; Research Institute of communication signal in China Academy of Railway Sciences: Beijing, China, 2014; pp. 1–52.



© 2018 by the authors. Licensee MDPI, Basel, Switzerland. This article is an open access article distributed under the terms and conditions of the Creative Commons Attribution (CC BY) license (<http://creativecommons.org/licenses/by/4.0/>).